Send Orders for Reprints to reprints@benthamscience.net

Current Nanomaterials, XXXX, *XX*, XX-XX

RESEARCH ARTICLE

Preparation, Optimization, and *In-Vitro* Release Study of Abemaciclib-Loaded Chitosan Nanocarrier as a New Approach for Breast Cancer Treatment

Mohanad Mohammed Ali[1], Samer Hasan Hussein-Al-Ali[1,2,*] and Mike Kh. Haddad[3]

[1]Department of Basic Pharmaceutical Sciences, Faculty of Pharmacy, Isra University, Amman 11622, Jordan; [2]Department of Chemistry, Faculty of Science, Isra University, Amman 11622, Jordan; [3]Department of Renewable Energy Engineering, Faculty of Engineering, Isra University, P.O. Box 22, Amman 11622, Jordan.

ARTICLE HISTORY

Received: October 21, 2023
Revised: December 26, 2023
Accepted: January 01, 2024

DOI:
10.2174/0124054615288714240110072000

Abstract: Abemaciclib (Abm) is a CDK inhibitor that specifically targets the CDK4/6 cell cycle pathway and has potential anticancer activity. Unfortunately, it has a low solubility and dissolution rate.

***Aim*:** The aim of this study is to enhance the solubility of ABM by loading it onto a chitosan (CS) polymer.

***Method*:** Polymer nanoparticle (NP) and Abm-CSNPs nanocomposites were prepared. Minitab 18 software was used to design 18 run samples to study the effects of CS, tripolyphosphate, and pH as independent variables on the loading efficiency and particle size (dependent variable). The response surface methodology (RSM) was also used to determine how the variables affected the response. The graphical analysis used surface plots, main effects plots, contour plots, and interaction graphs. The study includes F values, P values, variance inflation factors (VIFs), adjusted sums of square (Adj SSs), adjusted mean squares (Adj MSs) and square error of the coefficient (SE Coef). The carriers and loaded samples were also examined using the results of tests, including Fourier transform infrared spectroscopy, X-ray diffraction, and scanning electron microscopy. Furthermore, the release of Abm from Abm-CSNPs nanocomposite was studied in vitro.

***Results*:** The results revealed an ability to produce particle sizes ranging from (168-192) nm and loading efficiencies from (56.7-62.1).

***Conclusion*:** Abm-CSNPs nanocomposite may be used as an alternative drug delivery system for Abm to increase the release time of Abm to 1400 minutes.

Keywords: Abemaciclib, Optimization, Nanocomposites, Release Study.

1. INTRODUCTION

The most prevalent type of breast cancer in patients with early-stage and metastatic disease is hormone positive (HR+) breast cancer. Targeted CDK4 and CDK6 inhibitors have been discovered as a result of recent developments in our understanding of the pathophysiology of HR+ breast cancer. The three CDK4/6 inhibitors abemaciclib (Abm), ribociclib, and palbociclib were used that are readily available in the USA [1-3]. This class of medications appeals to both patients and medical professionals due to their manageable toxicity and oral administration. Abm has unique potential toxicities and pharmacologic properties [4].

Additionally, fulvestrant and Abm have been approved for the treatment of HER2-negative metastatic or advanced breast cancer in females whose disease has progressed after endocrine therapy (ET). Additionally, Abm has been approved for use in adults with metastatic disease who are progressing after ET but before receiving chemotherapy [5].

Abm has an absolute bioavailability of 45% and a distribution volume of approximately 690.3 L. It is water-insoluble (0.0159 mg/mL) [6].

Different medications have low bioavailability because they are poorly soluble in water. A drug must be specifically water soluble and have a reasonable level of bioavailability because water makes up about 65% of our bodies. Poorly water-soluble medications frequently leave the gastrointestinal tract (GIT) before they have a chance to fully dissolve and enter the bloodstream. This leads to low bioavailability and

*Address correspondence to this author at the Department of Basic Pharmaceutical Sciences, Faculty of Pharmacy, Isra University, Amman 11622, Jordan; E-mail: sameralali72@yahoo.com

2405-4615/XX $65.00+.00

poor dose proportionality, which highly hinders their clinical translations. Dose augmentation would be required in these circumstances to guarantee that the drug reaches the therapeutic concentration range in the blood. Following oral administration, this dose augmentation may occasionally result in topical toxicity in the GIT, which decreases patient compliance. A substantial amount of the active pharmaceutical ingredient would also raise the cost of creating and developing the drug product. In summary, drugs with low water solubility have detrimental clinical effects, including ineffective treatment, potentially dangerous interpatient variability issues, low bioavailability leading to ineffective drug delivery, higher patient costs, and higher risks of toxicity or death [7].

Poor water solubility of drugs limits their bioavailability and impedes pharmaceutical advancement. Drugs with poor aqueous solubility require the development of formulation layouts that are widely used across numerous methodologies, such as those used to increase the water solubility and slow the dissolution rate of BCS class II and IV drugs. For class II drugs in particular, there are a number of novel formulation options created for applications like co-solvents, and liposomal/noisomal formulations, melt granulation, change in pH, nanoparticle (NP) formation, cyclodextrin complexation, solubilization by salt formation, solid dispersion, supercritical fluid technology, co-crystallization and self-emulsification [8, 9].

Nanocomposites are increasingly being investigated for their various applications in medicine [10-13]. One of the fields with the most applications is drug delivery, where NPs can be used as carriers to deliver drugs to targeted sites by enhancing the solubility of drugs in different ways [14, 15]. NPs can encapsulate insoluble drugs within their core to form nanocomposites and protect the drug from degradation which improves their solubility [16-18].

NPs can also be used to form solid dispersions, in which the drug is dispersed or dissolved within a polymer matrix [19, 20]. This method enhances drug solubility by increasing the drug's surface area and reducing its crystallinity [21, 22].

Chitosan [CS] nanocomposites are one of the methods that have been extensively used to enhance the solubility of drugs [23, 24] due to their biocompatibility and biodegradable properties [25, 26]. By using CS nanocomposites, the surface area-to-volume ratio was enhanced and allowed for more efficient contact between the drug and the surrounding medium, promoting drug solubilization [27-29]. In addition, CS nanocomposites can disrupt the drug's crystalline structure, leading to increased drug surface exposure and faster dissolution in aqueous media [30, 31].

Sustained release refers to the controlled and prolonged release of a drug from a nanocarrier, leading to an extended period of time [32, 33]. It is a desirable property in many pharmaceutical formulations, leading to improved therapeutic efficacy [34, 35], reduced side effects [36, 37], improved pharmacokinetics [38-40], and targeted delivery [41, 42].

Our study aims to prepare polymer NP and Abm-CSNPs nanocomposites. The nanocomposites were characterized in terms of percent loading efficiency (%LE] and particle size. Furthermore, the benefits that can be gained by using the CS nanocomposites as a carrier system include the intercalation of cationic behaviors, the solubility of CS at the low pH of gastric fluid, which will decrease premature release of the drug in the gastric environment. The limited solubility of a CS–clay nanocomposite drug carrier at gastric pH offers significant advantages for colon-specific delivery because some drugs are destroyed in the stomach at acidic pH and in the presence of digestive enzymes. Based on the above, a CS nanocomposite drug carrier in the form of NPs was prepared to investigate the sustained release of a model cationic drug.

2. MATERIALS AND METHODS

2.1. Materials

Sodium hydroxide (NaOH) was purchased from Fischer, China. Abm ($C_{27}H_{32}F_2N_8$), low molecular weight CS, and sodium tripolyphosphate (TPP) were purchased from Sigma-Aldrich, USA. Acetic acid and dimethyl sulphoxide (DMSO) were purchased from SD fine-CHEM Limited, India.

2.2. Preparation of CSNPs

In a beaker, 1 ml of acetic acid was mixed with 100 ml of distilled water. Then, 50 mg of CS was added to the previous solution and stirred on a hot plate until it was completely dissolved (solution A). In another beaker, 50 mg of TPP was dissolved in 100 ml distilled water and stirred on a hot plate until it was completely dissolved to form solution B. Solution B was added dropwise to solution A, with continuous stirring. The CSNPs were stirred overnight and then refrigerated. The prepared CSNPs were dried in an oven at 40^{o}C [43, 44].

2.3. Preparation of Abm- CSNPs Nanocomposite

The solution of Abm was prepared by dissolving 0.1g of the drug in 30 ml of DMSO and then diluted by water. The solution of the drug was mixed with CS solution. The solution of TPP was added dropwise via a burette to the mixture solution of CS with the drug. The pH was adjusted using NaOH solution.

The Abm-CSNPs nanocomposite was stirred on a hot plate for 16 hours. After that, the nanocomposites were centrifuged at 11,000 rpm for 10 minutes. After centrifuge, the nanocomposites were washed with water and dried in an oven at 40^{o}C [45, 46].

2.4. Design of Experiments

In the present study, the statistical program Minitab was used to design 18 run samples to investigate the effects of independent variables (such as CS, TPP and pH) on the %LE and particle size by using the Placket-Burman experimental design [47, 48]. Table **1** summarizes the eighteen experimental trials, including the independent variables at higher and lower levels. The effects of the variables on the response were also determined using the response surface methodology (RSM) [49]. The graphical analysis used surface plots, main effects plots, contour plots, and interaction graphs. The study includes F values, P values, variance inflation factors (VIFs), adjusted mean squares (Adj MSs), adjusted sums of square (Adj SSs) and square error of the coefficient (SE Coef).

Table 1. CS, TPP weight used in sample preparation, and the pH of samples.

Sample	CS (mg)	TPP (mg)	pH
1	50	150	4.5
2	50	50	4.5
3	100	100	5.6
4	150	100	4.5
5	150	50	5.6
6	50	50	5.6
7	100	50	5.6
8	100	100	4.5
9	150	150	4.5
10	50	100	4.5
11	100	150	5.6
12	150	150	5.6
13	150	100	5.6
14	100	50	4.5
15	50	150	5.6
16	50	100	5.6
17	100	150	4.5
18	150	50	4.5

2.5. Determination of %LE of Abm in Abm-CSNPs nanocomposite

The %LE can be determined using Equation 1. The procedure was as follows:

1. The total amount of Abm was determined by the initial weight of the medication used to make each nanocomposite.

2. The weight of the free drug (unbound drug) was calculated in the supernatant after separating the nanocomposite using UV-Vis spectrophotometer at 360 nm, and a calibration curve:

$$\%LE = \frac{Q_T - Q_{un}}{\text{mass of nanocomposite}} \times 100 \qquad \text{Eq.1}$$

where Q_T is the total amount of Abm used in the experiments, Q_{un} is the unbound Abm that is present in the supernatant.

2.6. In vitro Release of Abm from the Nanocomposite

A UV-Vis spectrophotometer with a T_{max} 360 nm was used to determine the percentage of Abm released from the nanocomposites at pH 7.4 in a PBS solution. A proper amount of fine powder of the Abm-CSNPs nanocomposites was placed in the release media. Equation 2 was used to determine the percent release of Abm.

$$\%\ \text{Release} = \frac{\text{Concentration of Abm at time t}}{\text{Concentration of Abm in the nanocomposites}} \times 100 \qquad \text{Eq.2}$$

2.7. Experimental

UV-Vis spectrophotometry was used to measure the drug release with a Shimadzu UV-1601 spectrophotometer at Isra University. In addition, Fourier transform infrared spectroscopy (FTIR) was applied in the range of 400 and 4000 cm^{-1} on a Perkin Elmer with 4 cm^{-1} resolutions, with 0.01 g of sample. The particle size of the Abm-CSNPs nanocomposites was evaluated. Dynamic light scattering was performed with a Zetasizer (Malvern, UK). The powder X-ray diffraction (PXRD) technique was used in the range of 5-70° with an XRD D5005 diffractometer with CuKα radiation (Siemens, Munich, Germany). Scanning electron microscopy (FE-SEM) was done using a Zeiss LEO 1550 (Jena, Germany) instrument at ULM University.

2.8. Optimization of the Best Model

The instrument employs a current method for statistically designing an optimization of some recognized sets of independent components. To maximize profit and efficiency while minimizing costs, the number of trials was decreased to assess the advantage.

A collection of statistical and mathematical methods, known as RSM, are used to design experiments and optimize the effects of process factors based on the design of an experiment. RSM decreases the number of trials and demonstrates how the process parameters affect the removal process [50].

The formulations were improved in the current study using this optimization technique to achieve the maximum %LE, and smallest particle size.

2.9. Validation of Abm-CSNPs Nanocomposites

The validation procedure ensures that the analytical strategy used for a particular test is suitable for its intended application. A key component of good analytical practice is evaluating the accuracy, precision, and dependability of the analytical results using the results from the technique validation [51].

The validation model was used to evaluate the %LE and particle size percent biases to see if the expected values, actual values, and sufficient of those values were present. As validation samples, three random formulations with various component concentrations were employed (Table **2**).

Table 2. The optimized and validated sample formulation contents.

	CS (mg)	TPP (mg)	pH
Formulation 1	100	90.9	5
Formulation 2	129	78	5.2
Formulation 3	94	102	4.8

3. RESULTS AND DISCUSSION

To evaluate the variance between research variables, one-way ANOVA, and other statistical tests, including Minitab version 18.1, were used to examine the experimental data. The Plackett-Burman design, a different kind of statistical design, was employed. Table **3** displays the Plackett-Burman design matrix for the 18 trials and lab data used to examine %LE and particle size**.**

Table 3. Plackett-Burman design matrix to study %LE and particle size with 18 experiments.

Run Order	CS	TPP	pH	% LE	Size
1	50	150	4.5	*	269
2	50	50	4.5	69.0	256
3	100	100	5.6	77.0	208
4	150	100	4.5	45.0	*
5	150	50	5.6	41.4	270
6	50	50	5.6	85.0	*
7	100	50	5.6	77.0	280
8	100	100	4.5	54.0	*
9	150	150	4.5	58.0	260
10	50	100	4.5	43.0	200
11	100	150	5.6	64.0	*
12	150	150	5.6	76.0	323
13	150	100	5.6	*	243
14	100	50	4.5	55.0	204
15	50	150	5.6	*	297
16	50	100	5.6	*	220
17	100	150	4.5	47.0	*
18	150	50	4.5	15.0	189

The * in the table, as suggested by the software, refers to the removed data. The goal of this deletion is to raise R^2 value.

3.1. ANOVA values for %LE versus CS, TPP and pH

The ANOVA data for %LE is shown in Table 4; the %LE model shows linear variables (CS, TPP and pH), square (CS*CS and TPP*TPP) and 2-way interactions (CS*TPP, CS*pH and TPP*pH).

The F value and P value are techniques used in ANOVA analysis to compare two variances, indicate the significant relationship between them, and determine whether to accept or reject the null hypotheses. As a result, if the P value is low ($P < 0.05$), it will be noticeable in contrast to the high F value. The related P value is lower when the F value is higher. As seen in Table 4, all F values were high, and all the P values for the one-way interaction and two-way interactions were less than 0.05, except in CS, CS*pH and TPP*pH, which have a small F value and a higher related P value, indicating insignificant values.

The VIF in Table 4 represents multicollinearity; it shows mathematically how much the variance of the coefficients is inflated by the correlations between the predictors in the model. For example, the VIF of a regression on one model variable is equal to the ratio of the total model variance to the variance of the model containing only that single independent variable. A VIF number between 1 and 5 represents a moderate correlation, whereas a VIF value above 5.0 shows a significant correlation and is cause for interest. Table **4** showed VIF ranging from 1.13-2.06, which indicates moderate correlation (no multicollinearity).

The T value is a measurement of the magnitude of the difference relative to sample variability, calculated as the difference in standard error units. The higher the T value, the more proof that the null hypothesis is false [52].

According to this study's findings (shown in Table **4**), all the T values and the P values of the one and two-way interactions are significantly related to the %LE except for the considerable positive effect of CS, CS*pH, and the negative effect of TPP*pH due to large P value (0.358, 0.138 and 0.122, respectively) and T value closer to zero (1.01, 1.76 and -1.86, respectively).

R-squared (R^2) is a statistical measure used to show how much of a dependent variable's variance can be accounted for by one or more independent variables in a regression model. This number indicates how much the variance of one variable can be explained by the variance of another variable, R^2 [54]. $_{R}^2$ has several limitations for assessing the effects of independent variables on the correlation, even though it can be used to represent the degree of correlation with an index. The adjusted R^2 is helpful in measuring correlation in this situation.

The R^2 (adj) is a special form of R^2 that has been updated to account for the number of predictors in this model. When the additional term enhances the model beyond what would be predicted by chance, the R^2 (adj) increases. It will be reduced when a predictor results in a smaller model improvement than anticipated. The R^2 (adj) is typically less than the R^2. The R^2 value of a regression model tends to rise when more independent variables or predictors are included, which may entice one to include even more variables. Overfitting is what causes an unjustified high R^2 value to be produced.

Therefore, the predicted R-squared (R^2 (pred.)) determines how frequently this model will be accurate for future data when the R^2 (adj) can produce an accurate model that best fits the current data. These statistical measures have the following values in this study: R^2 = 99.52%, R^2 (adj) = 98.74%, and R^2 (pred.) = 95.74%.

3.2. ANOVA values for particle size (nm) versus CS, TPP and pH

The ANOVA data for particle size is shown in Table 5; the particle size model shows linear variables (CS, TPP and pH), square (CS*CS and TPP*TPP) and 2-way interactions (CS*TPP, CS*pH and TPP*pH).

Table 4. ANOVA values for %LE versus CS, TPP and pH.

	DF	Adj SS	Adj MS	F Value	P Value	Coef.	SE Coef	T value	VIF
Model	8	4572.05	571.51	128.31	0.000				
Linear	3	1337.81	445.94	100.12	0.000				
CS	1	4.55	4.55	1.02	0.358	1.10	1.09	1.01	2.06
TPP	1	171.30	171.30	38.46	0.002	-5.585	0.901	-6.20	1.77
pH	1	1032.44	1032.44	231.79	0.000	9.608	0.631	15.22	1.23
Square	2	500.40	250.20	56.17	0.000				
CS*CS	1	438.66	438.66	98.48	0.000	-13.35	1.35	-9.92	1.39
TPP*TPP	1	81.55	81.55	18.31	0.008	-5.85	1.37	-4.28	1.20
2-Way Interaction	3	1873.95	624.65	140.24	0.000				
CS*TPP	1	1822.15	1822.15	409.09	0.000	25.15	1.24	20.23	1.98
CS*pH	1	13.83	13.83	3.11	0.138	1.504	0.853	1.76	1.31
TPP*pH	1	15.41	15.41	3.46	0.122	-1.319	0.709	-1.86	1.13
Error	5	22.27	4.45						
Total	13	4594.32							
%LE	R^2=99.52%			R^2 (adj)=98.74%			R^2 (pre)=95.74%		
VIF = variance inflation factor, *Adj SS = adjusted sums of squares, *Adj MS = adjusted mean squares									

When employing a large number of independent variables in a regression, a set of numbers known as a coefficient is used to describe how much the dependent variables are expected to increase when one of the independent factors is raised while the other independent factors are held constant [53]. As seen in Table 4, CS*TPP has the most positive effect, CS (25.15), CS*pH (1.504) has non-significant positive effect, and the TPP*pH (-1.319) has the non-significant negative effect on %LE.

All F values were high except CS, and all of the P values for the one-way interaction were less than 0.05 except CS, indicating statistical significance. The interaction of CS*CS and TPP*pH suggests that there is no significant relationship because the F value is minimal, and the P value is more than 0.05.

CS has the lowest negative effect, while TPP*TPP has the highest positive significant effect, as indicated by the higher T value.

In this part of research, R^2 = 98.21%, R^2 (adj) = 94.64%, and R^2 (pred.) = 84.39%. A strong correlation between the dependent variable and the model is indicated by the value of R^2, which also suggests an excellent fit measure. The R^2 (adj) value demonstrated that the model is highly accurate and suitable for the current data; however, the R^2 (pred.) value was not even close to the anticipated R^2, suggesting that the model will not be accurate for the following data. Additionally, the VIF values fall between 1.11 and 1.4, indicating relations that are moderately linked.

3.3. Normal Probability Plot for %LE and Particle Size Model

By showing the sorted data vs. an approximation of the means using the vertical and horizontal axes, the normal probability is a graphical technique. The percentiles are determined, and the sample distributions are compared using a probability map to see how well a distribution fits the data. A probability plot displays each value against the percentages of the sample values that are less than or equal to it further along the fitted distribution line. Next, a straight line is created by converting the fitted distribution along the y-axis [55].

Tables **4** and **5**, respectively, provide the R^2 values for the %LE and particle size models. These high values suggested that %LE and particle size were plotted in a straight line. The best straight line was found in %LE. Fig. (**1**) shows the normal probability plot for %LE and particle size. All residual values are found close to the normality line, indicating that the residuals were normally distributed.

3.4. Residual Plots for %LE and Particle Size Models

The distribution of the data was examined using the normal probability plot of residuals. It is recommended that the residual plot approach should follow a straight line.

The residual plot is a graph used to assess the quality of fit in ANOVA and regression. It is helpful to look at residual plots to determine whether the usual least-squares assumptions are being upheld. If these suspicions are confirmed, normal least-squares relapse will produce fair coefficient gauges with the basic difference [56-58].

Table 5. ANOVA values for particle size (nm) versus CS, TPP and pH.

-	DF	Adj SS	Adj MS	F Value	P Value	Coef.	SE Coef	T value	VIF
Model	**8**	**19948.2**	**2493.5**	**27.48**	**0.003**	-	-	-	-
Linear	3	11300.0	3766.7	41.51	0.002	-	-	-	-
CS	1	553.4	553.4	6.10	0.069	-8.20	3.32	-2.47	1.22
TPP	1	1689.0	1689.0	18.62	0.013	16.27	3.77	4.31	1.40
pH	1	7416.0	7416.0	81.74	0.001	27.10	3.00	9.04	1.28
Square	2	10872.8	5436.4	59.92	0.001	-	-	-	-
CS*CS	1	435.2	435.2	4.80	0.094	15.91	7.26	2.19	1.34
TPP*TPP	1	10599.5	10599.5	116.82	0.000	67.80	6.27	10.81	1.20
2-Way Interaction	3	3155.0	1051.7	11.59	0.019	-	-	-	-
CS*TPP	1	1122.8	1122.8	12.38	0.024	13.94	3.96	3.52	1.20
CS*pH	1	1211.7	1211.7	13.35	0.022	11.78	3.22	3.65	1.11
TPP*pH	1	225.8	225.8	2.49	0.190	-5.33	3.38	-1.58	1.12
Error	4	362.9	90.7	-	-	-	-	-	-
Total	12	20311.1	-	-	-	-	-	-	-
Particle size	**R^2=98.21%**			**R^2 (adj)= 94.64%**			**R^2 (pred.)= 84.39%**		

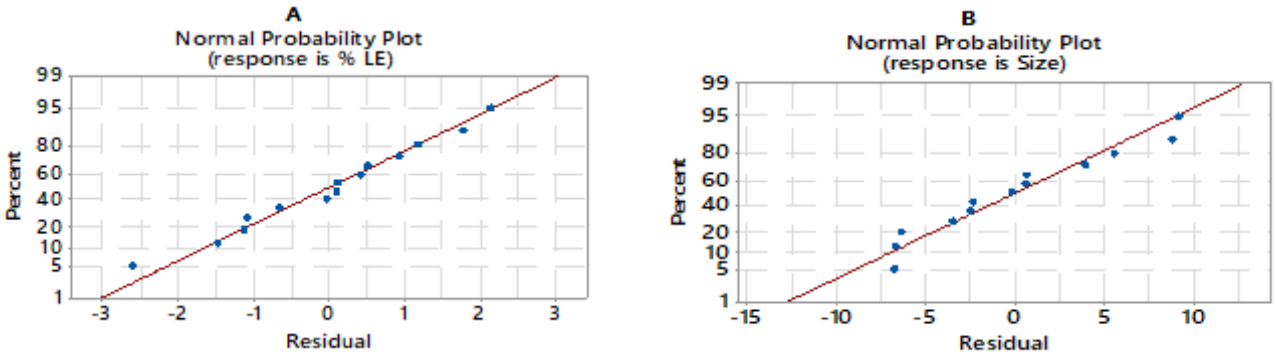

Fig. (1). Normal probability plot for (**A**) %LE and (**B**) particle size.

In this study, the %LE and particle size residuals vs. fits plots show no regular pattern, according to the data. In other words, since the number of dots above the line is almost equal to the number of dots below the line, the model did not contain any systematic probability mistakes as seen in Fig. (**2**).

3.5. Impact of Pareto Charts on %LE and Particle Size

Pareto charts determine the statistically significant influence among various effects based on the curve graph and the magnitude order of the data, from greatest to smallest. In this graph, statistically significant effects are represented by the columns that cross the red line (Fig. **3**).

Referring to Fig. (**3A**) for %LE, the Pareto chart displays the bars for TPP and pH as well as their interactions with other variables (TPP*TPP, CS*CS, and CS*TPP), all of which cross the reference line at point (2.57). The results show that these variables had a significant impact on %LE (at a P-level of 0.05). The effect of CS*TPP was the most highly significant, followed by CS*CS and TPP*TPP, in that order. The %LE, however, was not significantly influenced by CS, CS*pH, or TPP*pH.

The bars for the TPP and pH variables, as well as their interactions with other variables, crossed the red line at the point (2.78) for the particle size aspect, as shown in Fig. (3-B). This demonstrates that these factors significantly affected the particle size statistically (at a P-level of 0.05). TPP*TPP had the greatest impact, followed by pH, TPP, CS*pH, and CS*TPP, in that order. This shows that these variables had an impact on particle size that was statistically significant. The particle size, however, was not significantly influenced by CS, CS*CS, or TPP*pH.

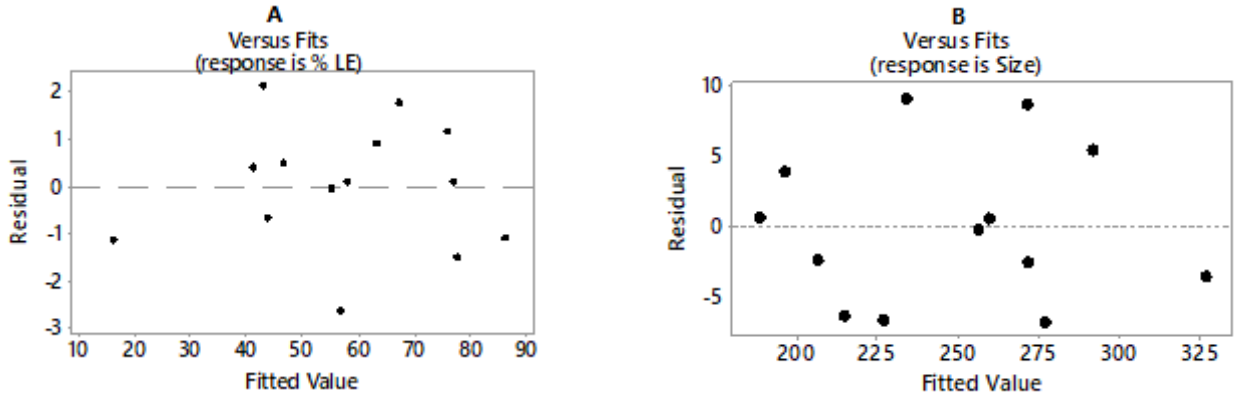

Fig. (2). Residual vs. data fitted values for (**A**) %LE and (**B**) particle size.

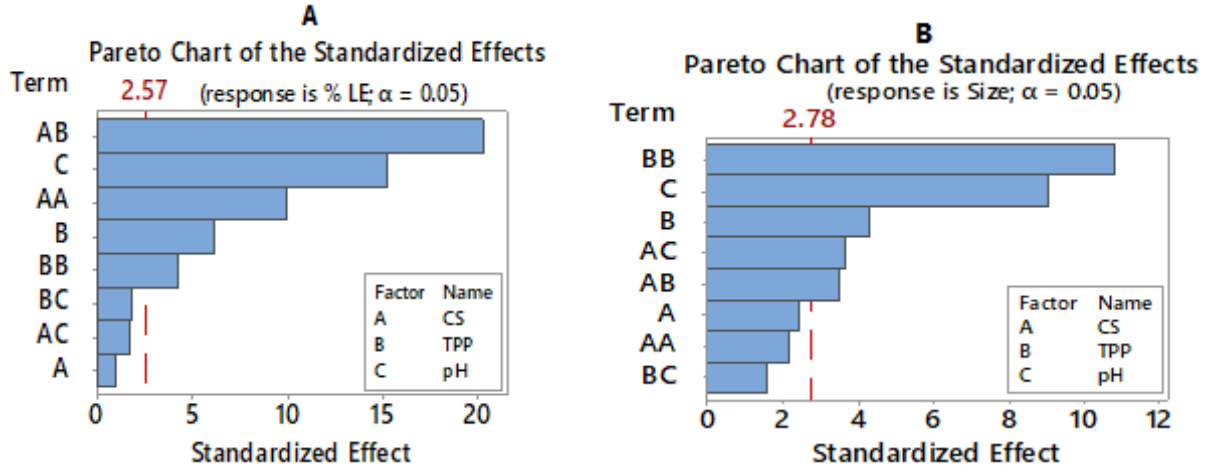

Fig. (3). Impact of Pareto chart on %LE and particle size.

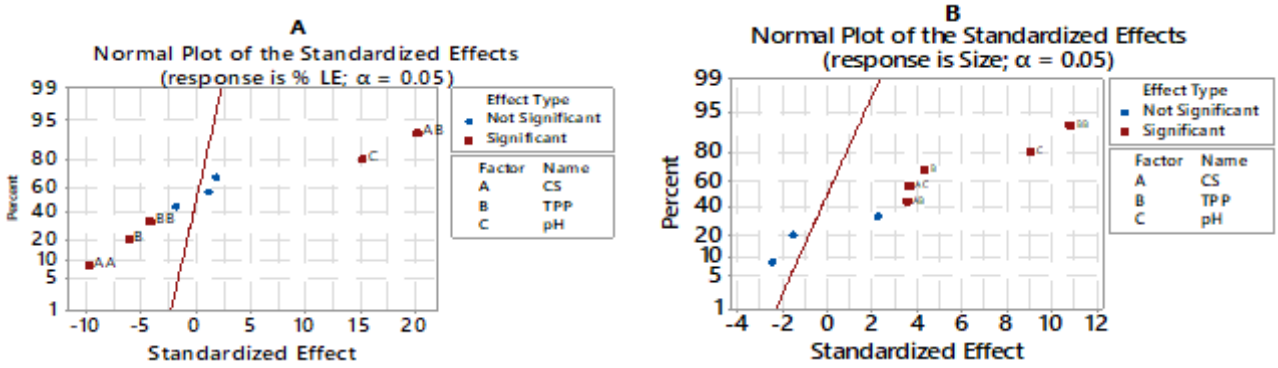

Fig. (4). Normal probability plot of (**A**) %LE and (**B**) particle size.

3.6. Normal Plot of the Standardized Effect

The normal plot of the effects was used to determine the magnitudes, orientations, and significance of the impacts. Effects on the normal plot that deviate further from 0 are statistically significant. The color and shape of the points differ between statistically significant and statistically insignificant impacts. In terms of color and shape, these points are distinct from the points for insignificant impacts.

A favorable standardized effect on the right side is indicated by the red points. When a component shifts from a low to a high level, the effect increases, and the response follows. Additionally, the figure shows the effect's direction. The blue points represent negative standardized impacts. The response diminishes as the effect increases. As seen in Fig. (**4**), the normal plot shows all the variables that have P values less than 0.05 as significant and scattered from 0.

Since their data points deviate further from the line and have substantial positive effects, Fig. (**4A**) reveals that CS*TPP has the most significant positive effect on %LE followed by pH; this means the effect rises as the response increases. Additionally, CS*CS, TPP and TPP*TPP exhibit

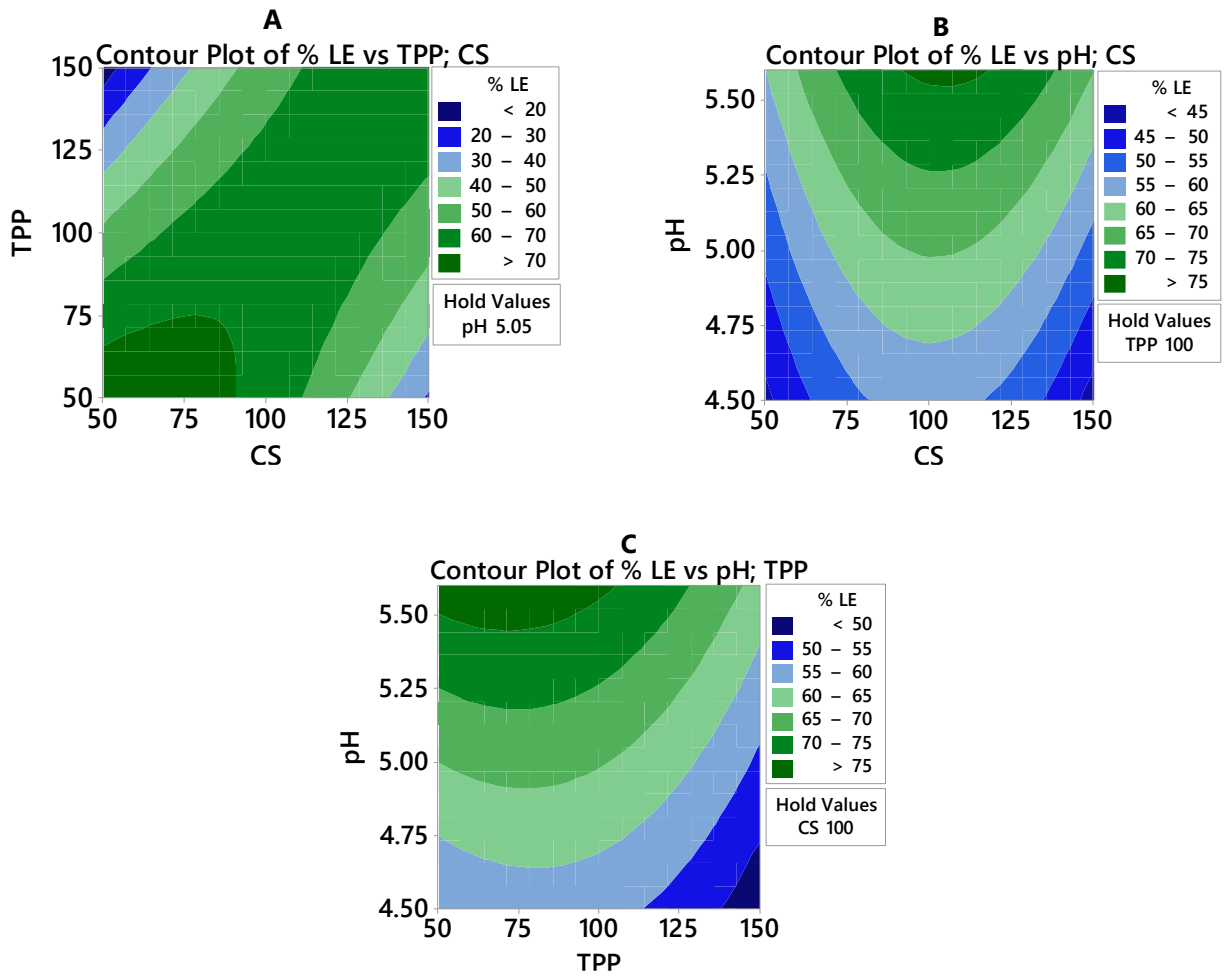

Fig. (5). Counter plot of %LE against (A)TPP; CS, (B) pH; CS, and (C) pH; TPP.

significant negative effects on %LE; when these factors increase, the response decreases.

In Fig. (**4B**), there is no negative significant effect. TPP*TPP shows the most significant positive effect on particle size followed by pH, TPP, CS*pH and CS*TPP, respectively. This means the effect increases as the response increases.

3.7. Contour Plots of the Impacts of %LE and Particle Size

The %LE responses against the TPP; CS, pH; CS, pH; TPP variables are shown in Fig. (**5**). As indicated in Fig. (**5A**), to achieve more than 70% %LE, the concentration of the TPP should be <70, and the concentration of CS should be <90 when holding the values of pH at 5.05. While in Fig. (**5B**) to achieve 70-75 %LE, the pH should be > 5.3, and the concentration of CS should be 75-135, while holding the value of TPP at 100. Also, to achieve more than 75% %LE, the pH should be > 5.6 and the concentration of CS should be 90-110 while holding the value of TPP at 100. Fig. (**5C**) shows that to achieve a %LE higher than 75, the pH should be > 5.45 and the concentration of TPP should be 50-110, while holding the value of CS at 100.

The particle size responses against the TPP; CS, pH variables are shown in Fig. (**6**). Fig. (**6A**) indicates that the minimum particle size was less than 200 nm. The response was achieved at a TPP concentration of (70-110), and the concentration of CS was (70-150) while holding the pH at 5.05. As shown in Fig. 6-B, the minimum particle size of less than 160 nm was achieved at a pH of(<5.57), and the concentration of CS was (100-150) while holding the TPP at 100. In Fig. (**6C**), the minimum particle size was less than 160 nm, which was achieved at a pH of (<4.6) and a concentration of TPP of (90-100) while holding the CS at 100.

3.8. Main Effect Plots for %LE and Particle Size

To study the variations in factor-level means for one or more factors, main effect plots were developed. When different component levels have an impact on the response, it has a significant impact. Each response indicates that in the main effect plots, a shown line corresponds to each factor level.

When the main effect line is parallel to the x-axis, there is no factor interaction. The means of the responses are the same for all levels of the factor, and each level of the factor has the same impact on the response. When the line is not parallel, there is a significant impact. Varied effects are influenced

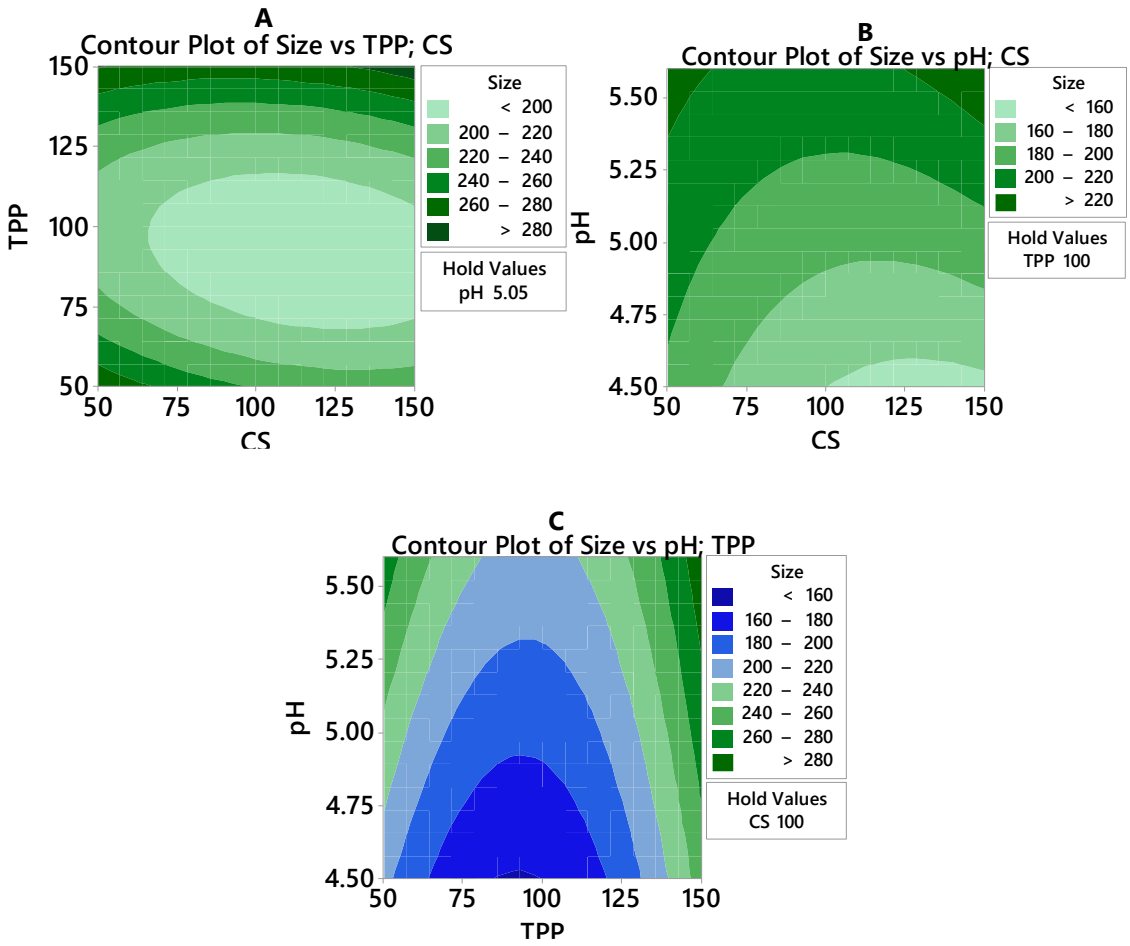

Fig. (6). Counter plot of size against (**A**) TPP; CS, (**B**) pH; CS, and (C) pH; TPP.

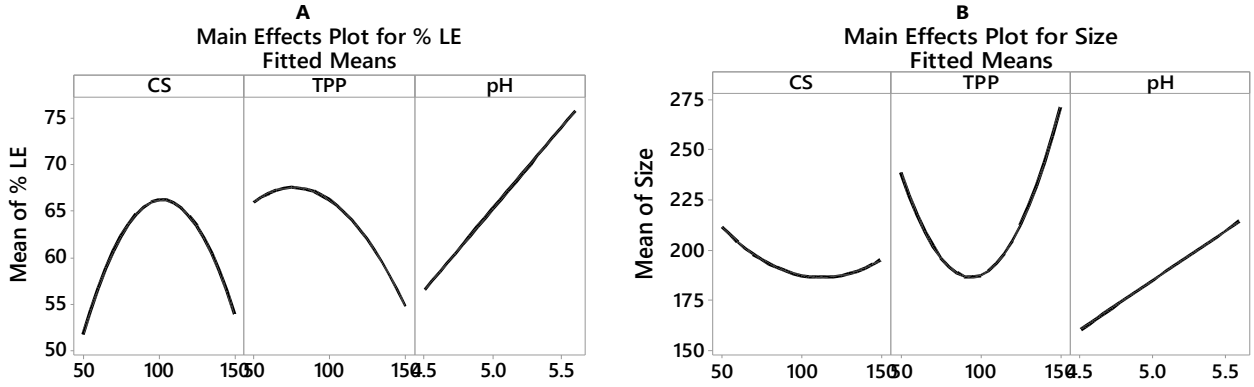

Fig. (7). Main effect plot for (**A**) %LE and (**B**) particle size.

differently by different amounts of the component. The slope of the line directly relates to the size of the main effect.

Fig. (**7A**) shows that by increasing the concentration of CS, the mean %LE tends to increase until it reaches a concentration of 100, then the mean %LE starts to decrease. In TPP, the mean %LE tends to increase until reaches a concentration of 75, then it starts to decrease. An effect on the mean %LE was noticed for the pH which shows a positive slope, indicating that the mean %LE increases as the concentration increases.

The main effect plot for size (Fig **7-B**) shows a decrease in mean size with an increase in the concentration of CS at a non-constant rate. In TPP, the mean %LE tends to decrease until it reaches a concentration of 100, then it starts to increase. The pH shows a positive slope, indicating that the mean %LE increases as the concentration increases.

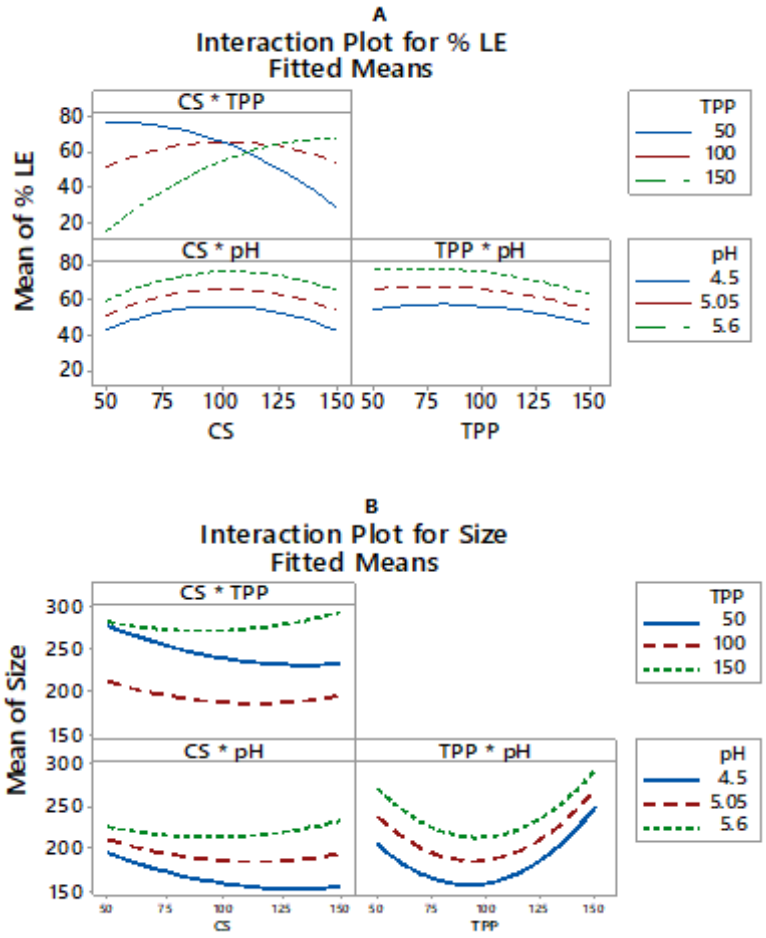

Fig. (8). Interaction plot for (**A**) %LE and (**B**) particle size.

Table 6. Regression values for %LE and particle size.

Regression Model Equations	
%LE	%LE=14.2 - 0.192 CS - 0.408 TPP + 16.80 pH - 0.005342 CS*CS - 0.002339 TPP*TPP + 0.010061 CS*TPP + 0.0547 CS*pH - 0.0480 TPP*pH
Size	Size=431.4 - 4.158 CS - 4.677 TPP + 25.8 pH + 0.00636 CS*CS + 0.02712 TPP*TPP + 0.00558 CS*TPP + 0.428 CS*pH - 0.194 TPP*pH

3.9. Interaction Plots for %LE and Particle Size

In this research, interaction plots were utilized to track any potential interactions where one component's effect was in some way influenced by another component's degree of influence. Each plot has an additional line that represents numerous elements at various levels and an x-axis with varying values of one influencing element. When displayed as parallel lines, there is no discernible interaction between the research variables. In other words, there is more interaction when there is a larger slope difference between two lines.

Fig. (**8-A**) shows that there is a significant interaction between CS and TPP (lines are not parallel), while in the CS with pH, and TPP with pH relationships, an insignificant interaction was found (parallel lines). Fig. (**8-B**) shows that there is a significant interaction between CS with TPP and CS with pH and a non-significant interaction between TPP and pH.

3.10. Regression equation for %LE and particle size models

In this study, two regression equations were obtained after mathematically analyzing the experimental data (Table **6**). The %LE and particle size can be obtained from this equation.

3.11. Optimization of %LE and Particle Size Models

A current approach to optimize some specified sets of dependent factors is by using a tool that optimizes the process by statistical design (response). This conserves costs while enhancing revenue and effectiveness [59].

A small number of predictors were optimized using the optimization method, which was used to perform and measure response surface design (RSD) [60].

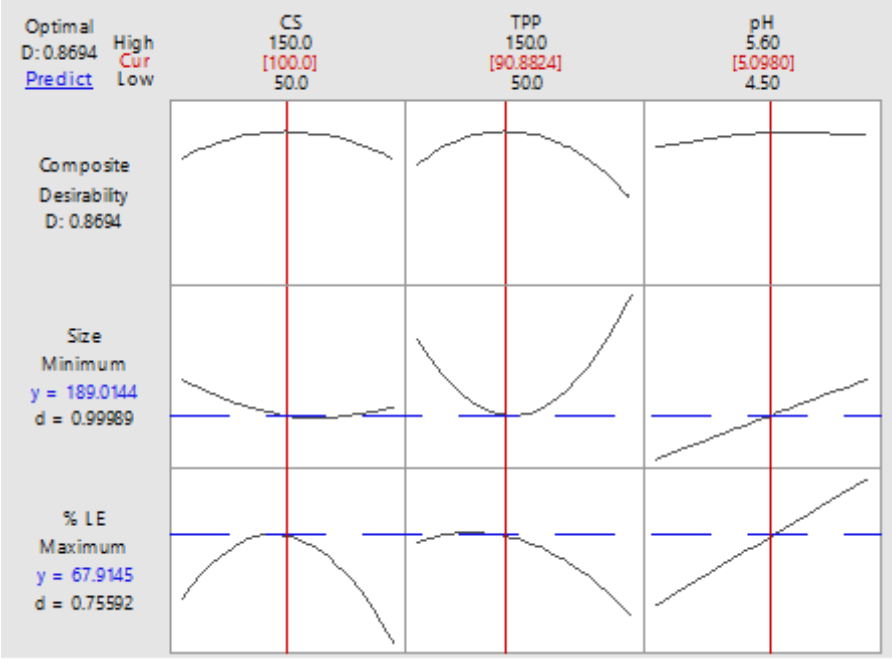

Fig. (9). Optimization conditions for %LE and particle size models.

Table 7. Summary of validation parameters for %LE, and particle size model.

Concentrations	Experimental Response	Predicted Values	Observed Values	Bias (%)
CS (100 mg) TPP (90.9 mg) pH (5.0)	%LE	67.9	62.1	-8.5
	Particles Size (nm)	189±7	180±9	-4.8
CS (129 mg) TPP (78 mg) pH (5.2)	%LE	59.5	56.7	-4.7
	Particles Size (nm)	197±10	192±15	-2.5
CS (94 mg) TPP (102 mg) pH (4.8)	%LE	60.9	59.2	-2.8
	Particles Size (nm)	177±22	168±45	-5.1
((Observed value - Predicted value) / Predicted value) x100 was used to calculate the percentage of bias.				

The equations in Table **4.4** show the %LE and particle size. The optimized formula can be deduced for the highest %LE and smallest particle size. This formula can be achieved by using 100 mg of CS, 90.8824 mg of TPP, and 5.098 mg of pH (Fig. **9**). This formula has a %LE of 67.9145% and a particle size of 189.0144 nm.

3.12. Validation of the Three Models

Method validation is proof of how precise the procedures and results are. One technique used to evaluate the validity is the value of bias. The comparison of the observed and predicted values of the variables for the %LE and particle size models is shown in Table **7**.

The values of bias were -8.5 (%LE) and -4.8 (particle size) for the sample which was composed of CS (100 mg), TPP (90.9 mg) with a pH of (5.0). For the second sample, CS (129 mg), TPP (78 mg) and a pH value of (5.2) were employed, and the values of bias were -4.7 and -2.5 for %LE and particle size, respectively. Also, for the third sample, CS (94 mg), TPP (102 mg) and a pH value of (4.8) were used, and the values of bias were -2.8. and -5.1 for %LE and particle size, respectively. These results prove the validity and accuracy of the models that were used in this study because the predicted values were close to the observed value.

4. CHARACTERIZATION

4.1. X-ray Diffraction Analysis (XRD)

The results of the XRD examination revealed the presence of distinctive diffraction peaks of CSNPs (Fig **10B**). From the literature, normal CS shows a strong diffraction peak at around 20.1°, which is due to (001) and (100) planes that belong to the monoclinic system, in addition to one more weak

diffraction peak at 10.6 [61]. The XRD pattern of the CSNPs revealed large, characteristic diffraction peaks at 2θ values of 19.85 [62]. Comparing this result with the XRD spectrum of CS powder, the 10° diffraction peak disappeared completely, the 20° diffraction peak's relative intensity decreased significantly, and the amorphous area relatively increased. This is because the process of milling disrupts the crystalline regions of CS and produces highly amorphous NPs [63]. XRD of Abm (Fig. **10A**) exhibited various characteristic sharp and intense peaks at 6.00° (2θ), 6.80° (2θ), 12.00° (2θ), 15.40° (2θ), 18.60° (2θ), 21.00° (2θ) and 26.2° (2θ), as reported in literature [64, 65].

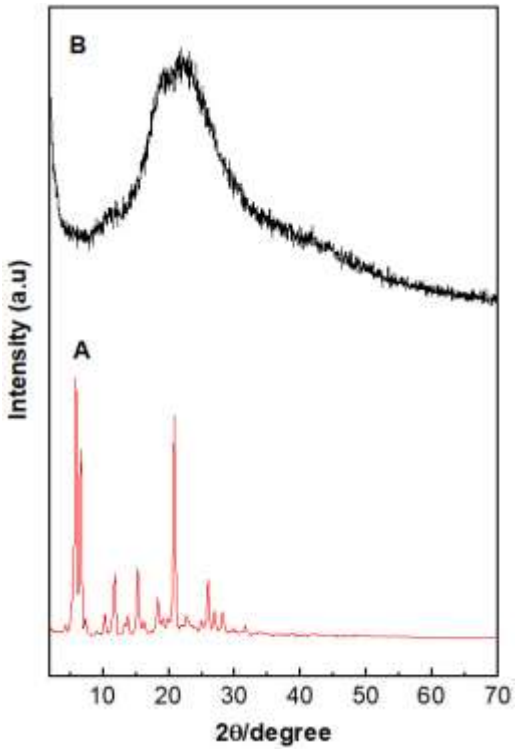

Fig. (10). XRD for Abm (**A**) CSNPs (**B**).

4.2. Fourier transform Infrared (FT-IR)

Fig. (**11A-C**) shows the FTIR spectra for Abm, CS, and Abm-CSNPs nanocomposite, respectively. FTIR spectra of Abm are shown in Fig. (**11A**). The peaks 3500 cm^{-1}, 3100 cm^{-1}, 2900-2800 cm^{-1}, 1600 cm^{-1} and 1500 cm^{-1} are attributed to amine, C-H (Sp2), C-H (Sp3) stretching, C=C bond and C-X (halogen), respectively. Also, C-N bond appears in the fingerprint region at 1300 cm^{-1} [64, 66]. In (Fig. **11B**) for CS, the peak at 3447 cm-1 is attributed to $–NH_2$ groups stretching vibration. The peak at 1650 cm^{-1} is attributed to the $CONH_2$. Characteristics of CS are consistent with the literature reported data (67].

The FTIR spectra of the Abm-CSNPs nanocomposites are shown in Fig. (**11C**). The superimposition of peaks of CS and peaks of Abm in the spectra indicates that Abm is present in the Abm-CSNPs nanocomposites.

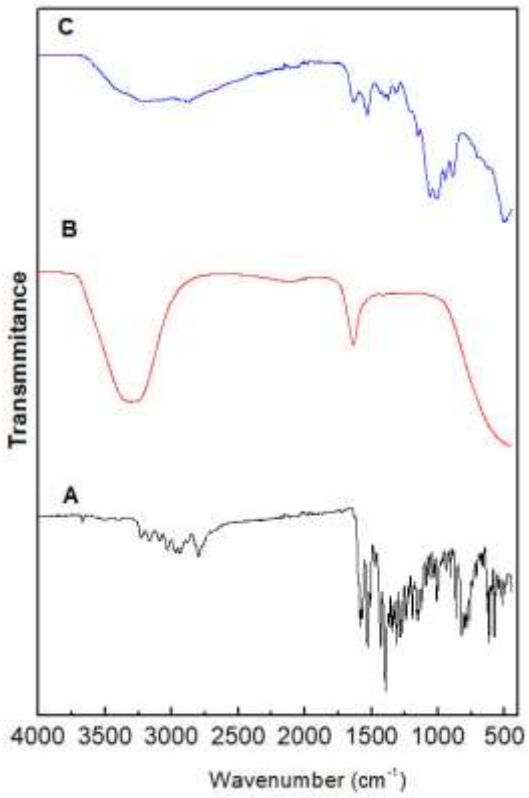

Fig. (11). FTIR spectrum for Abm (**A**), CS (**B**), and Abm-CSNPs nanocomposite (**C**).

4.3. The Interaction between Abm and CSNPs in Abm-CSNPs Nanocomposites

CS with a pKa of 6.3 is polycationic when dissolved in acid and presents $–NH_3^+$ sites. In addition, TPP dissolved in water gives both hydroxyl and phosphoric ions [68]. Therefore, the CSNPs contain ionic interaction behaviors. The pH used in this work was in the range 4.5-5.6, which means that the Abm has a positive charge. This also indicates ionic interaction behaviors between TPP and Abm (Fig. **12**).

4.4. Scanning electron microscopy (SEM)

Focused electron beams are used in SEM to produce high-resolution, three-dimensional images. These pictures reveal details about composition, morphology, and topography. The SEM image of Abm-CSNPs nanocomposite is shown in Fig (**13**). As can be seen, Abm-CSNPs nanocomposite is almost spherical [69].

4.5. *In Vitro* Release Study of Abm from Abm-CSNPs Nanocomposites

The release profile curves of Abm from the Abm-CSNPs nanocomposites are shown in Fig. (14). The release curves are from zero time to 1400 minutes. Abm release from the Abm-CSNPs nanocomposites occurs in direct relationship with time (percent release of drug increases as time increases) uptp 1400 minutes.

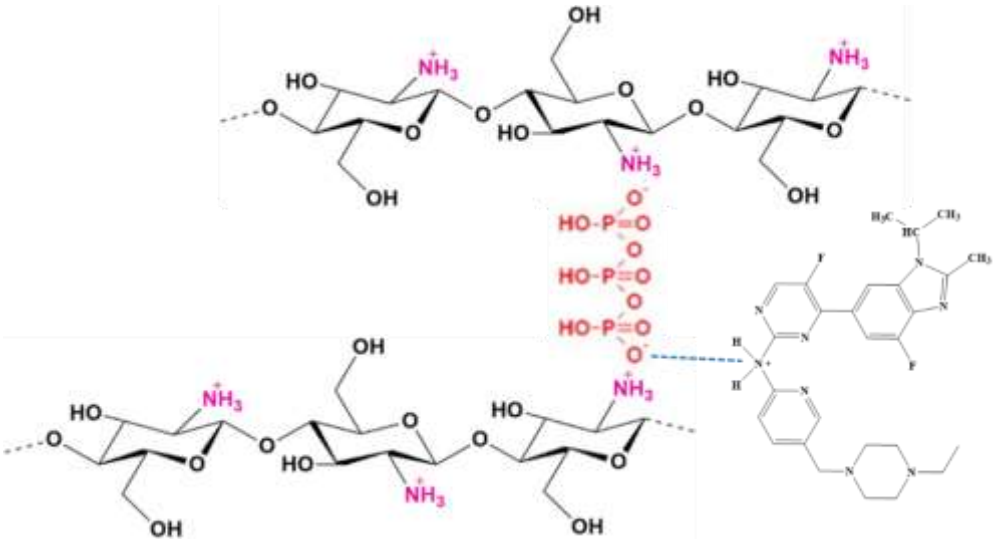

Fig. (12). Interaction of CS with TPP and Abm in Abm-CSNPs nanocomposites.

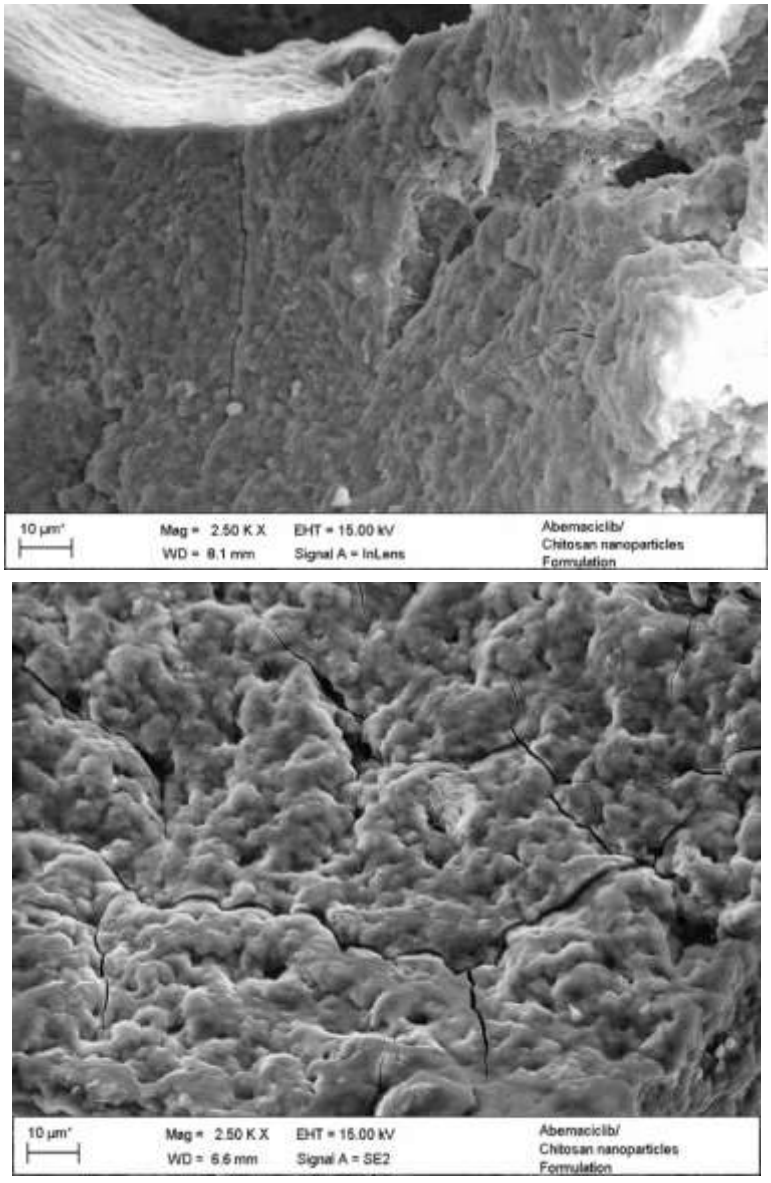

Fig. (13). The SEM image of Abm-CSNPs nanocomposite.

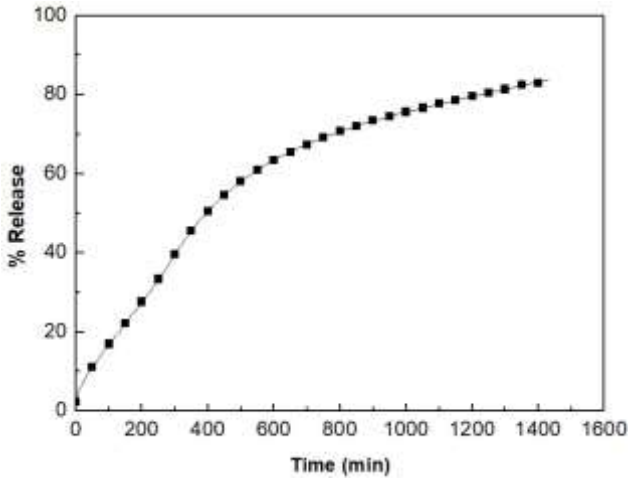

Fig. (14). The release profile curves of Abm from the Abm-CSNPs nanocomposites.

CONCLUSION

In conclusion, Abm-CSNPs nanocomposites were produced in this study. The software Minitab 18.1 was used to study the effect of the independent variables (such as CS, TPP and pH) on the %LE and particle size. The results revealed an ability to produce particle sizes ranging from (168-192) nm and %LE ranging from (56.7-62.1). FTIR was performed to determine the functional groups of the Abm-CSNPs nanocomposites formulation and to explain the interaction between Abm and Abm-CSNPs nanocomposites. Furthermore, an Abm-CSNPs nanocomposite was used as an alternative drug delivery system for Abm to increase the release time to 1400 minutes.

ETHICS APPROVAL AND CONSENT TO PARTICIPATE

Not applicable.

HUMAN AND ANIMAL RIGHTS

Not applicable.

CONSENT FOR PUBLICATION

Not applicable.

AVAILABILITY OF DATA AND MATERIALS

Data are available on request from the corresponding author Dr. Samer Hasan Hussein-Al-Ali.

FUNDING

The study was funded by the Faculty of Pharmacy at Isra University for providing funding for this research under grant number 2021/2022/2/21.

CONFLICT OF INTEREST

The authors declare no conflict of interest, financial or otherwise.

ACKNOWLEDGEMENTS

The author would like to thank the Faculty of Pharmacy at Isra University for providing funding for this research under grant number 2021/2022/2/21. Furthermore, the authors would like to acknowledge the Institute of Functional Nanosystems for permission to use their advanced facilities at ULM University (Germany).

REFERENCES

[1] Basati G, Saffari-Chaleshtori J, Abbaszadeh S, Asadi-Samani M, Ashrafi-Dehkordi K. Molecular dynamics mechanisms of the inhibitory effects of abemaciclib, hymenialdisine, and indirubin on CDK-6. Curr Drug Res Rev 2019; 11(2): 135-41. http://dx.doi.org/10.2174/2589977511666191018180001 PMID: 31875784

[2] Sammons SL, Topping DL, Blackwell KLHR. +, HER2-advanced breast cancer and CDK4/6 inhibitors: mode of action, clinical activity, and safety profiles. Curr Cancer Drug Targets 2017; 17(7): 637-49. PMID: 28359238

[3] Ates-Alagoz Z, Hassan MA-K. Cyclin-dependent kinase 4/6 inhibitors against breast cancer. Mini Rev Med Chem 2023; 23(4): 412-28. http://dx.doi.org/10.2174/1389557522666220606095540 PMID: 35670349

[4] Martin JM, Goldstein LJ. Profile of abemaciclib and its potential in the treatment of breast cancer. OncoTargets Ther 2018; 11: 5253-9. http://dx.doi.org/10.2147/OTT.S149245 PMID: 30214230

[5] Kim ES. Abemaciclib: First global approval. Drugs 2017; 77(18): 2063-70. http://dx.doi.org/10.1007/s40265-017-0840-z PMID: 29128965

[6] Ansarinik Z, Kiyani H, Yoosefian M. Investigation of self-assembled poly(ethylene glycol)-poly(L-lactic acid) micelle as potential drug delivery system for poorly water soluble anticancer drug abemaciclib. J Mol Liq 2022; 365: 120192. http://dx.doi.org/10.1016/j.molliq.2022.120192

[7] Kakran M, Li L, Müller RH. Overcoming the challenge of poor drug solubility. Pharm Eng 2012; 32(4): 1-7.

[8] Chowdary K. Recent research on formulation development of BCS class II drugs–A review. Int Res J Pharm Appl Sci 2013; 3(1): 173-81.

[9] Kawabata Y, Wada K, Nakatani M, Yamada S, Onoue S. Formulation design for poorly water-soluble drugs based on biopharmaceutics classification system: Basic approaches and practical applications. Int J Pharm 2011; 420(1): 1-10. http://dx.doi.org/10.1016/j.ijpharm.2011.08.032 PMID: 21884771

[10] Buniyamin I, Akhir RM, Asli NA, Khusaimi Z, Malek MF, Mahmood MR. Nanotechnology applications in biomedical systems. Curr Nanomater 2022; 7(3): 167-80. http://dx.doi.org/10.2174/2405461507666220301121135

[11] Sarmah P, Choudhary B. Nanomaterials for targeted delivery of anticancer drugs: An overview. Curr Nanomater 2022; 7(1): 31-9. http://dx.doi.org/10.2174/2405461506666210119095130

[12] Mehata AK, Dehari D, Gupta A, Rabin DC, Miya A. Multifunctional liquid crystal nanoparticles for cancer therapy. Curr Nanomater 2021; 6(1): 4-16. http://dx.doi.org/10.2174/2405461506666210118114851

[13] Jha S, Malviya R. Role of nanostructured biomaterials in the treatment and diagnosis of biological disorder. Curr Nanomater 2021; 6(1): 23-30. http://dx.doi.org/10.2174/2405461505999201027214348

[14] Yusuf A, Almotairy ARZ, Henidi H, Alshehri OY, Aldughaim MS. Nanoparticles as drug delivery systems: A review of the implication of nanoparticles' physicochemical properties on responses in biological systems. Polymers 2023; 15(7): 1596. http://dx.doi.org/10.3390/polym15071596 PMID: 37050210

[15] Begum MY. Advanced modeling based on machine learning for evaluation of drug nanoparticle preparation *via* green technology:

Theoretical assessment of solubility variations. Case Stud Therm Eng 2023; 45: 103029.
http://dx.doi.org/10.1016/j.csite.2023.103029

[16] Wais U, Jackson AW, He T, Zhang H. Nanoformulation and encapsulation approaches for poorly water-soluble drug nanoparticles. Nanoscale 2016; 8(4): 1746-69.
http://dx.doi.org/10.1039/C5NR07161E PMID: 26731460

[17] Guo S, Huang L. Nanoparticles containing insoluble drug for cancer therapy. Biotechnol Adv 2014; 32(4): 778-88.
http://dx.doi.org/10.1016/j.biotechadv.2013.10.002 PMID: 24113214

[18] Wei W, Lu M, Xu W, Polyakov NE, Dushkin AV, Su W. Preparation of protamine-hyaluronic acid coated core-shell nanoparticles for enhanced solubility, permeability, and oral bioavailability of decoquinate. Int J Biol Macromol 2022; 218: 346-55.
http://dx.doi.org/10.1016/j.ijbiomac.2022.07.152 PMID: 35878671

[19] Kong Y, Wang W, Wang C, Li L, Peng D, Tian B. Supersaturation and phase behavior during dissolution of amorphous solid dispersions. Int J Pharm 2023; 631: 122524.
http://dx.doi.org/10.1016/j.ijpharm.2022.122524 PMID: 36549404

[20] Correa Soto CE, Gao Y, Indulkar AS, Ueda K, Zhang GGZ, Taylor LS. Impact of surfactants on the performance of clopidogrel-copovidone amorphous solid dispersions: Increased drug loading and stabilization of nanodroplets. Pharm Res 2022; 39(1): 167-88.
http://dx.doi.org/10.1007/s11095-021-03159-w PMID: 35013849

[21] Yadav K, Sachan AK, Kumar S, Dubey A. Techniques for increasing solubility: A review of conventional and new strategies. Asian J Pharm Res Dev 2022; 10(2): 144-53.
http://dx.doi.org/10.22270/ajprd.v10i2.1054

[22] Huang H, Zhang Y, Liu Y, Guo Y, Hu C. Influence of intermolecular interactions on crystallite size in crystalline solid dispersions. Pharmaceutics 2023; 15(10): 2493.
http://dx.doi.org/10.3390/pharmaceutics15102493 PMID: 37896253

[23] Khushbu JR, Jindal R. Thermal stability and optimization of graphene oxide incorporated chitosan and sodium alginate based nanocomposite containing inclusion complexes of paracetamol and β-cyclodextrin for prolonged drug delivery systems. Polym Bull 2023; 80(2): 1751-72.
http://dx.doi.org/10.1007/s00289-022-04157-7

[24] kapoor D, Garg R, Gaur M, *et al.* Polymeric nanoparticles approach and identification and characterization of novel biomarkers for colon cancer. Results Chem 2023; 6: 101167.
http://dx.doi.org/10.1016/j.rechem.2023.101167

[25] Zou Y, Yue P, Cao H, *et al.* Biocompatible and biodegradable chitin-based hydrogels crosslinked by BDDE with excellent mechanical properties for effective prevention of postoperative peritoneal adhesion. Carbohydr Polym 2023; 305: 120543.
http://dx.doi.org/10.1016/j.carbpol.2023.120543 PMID: 36737194

[26] Mukherjee C, Varghese D, Krishna JS, *et al.* Recent advances in biodegradable polymers – Properties, applications and future prospects. Eur Polym J 2023; 192: 112068.
http://dx.doi.org/10.1016/j.eurpolymj.2023.112068

[27] Pathak R, Bhatt S, Punetha VD, Punetha M. Chitosan nanoparticles and based composites as a biocompatible vehicle for drug delivery: A review. Int J Biol Macromol 2023; 253(Pt 7): 127369.
http://dx.doi.org/10.1016/j.ijbiomac.2023.127369 PMID: 37839608

[28] Herdiana Y, Husni P, Nurhasanah S, Shamsuddin S, Wathoni N. Chitosan-based nano systems for natural antioxidants in breast cancer therapy. Polymers 2023; 15(13): 2953.
http://dx.doi.org/10.3390/polym15132953 PMID: 37447598

[29] Mohite P, Rahayu P, Munde S, *et al.* Chitosan-based hydrogel in the management of dermal infections: A review. Gels 2023; 9(7): 594.
http://dx.doi.org/10.3390/gels9070594 PMID: 37504473

[30] Kumar V, Sharma N, Janghu P, *et al.* Synthesis and characterization of chitosan nanofibers for wound healing and drug delivery application. J Drug Deliv Sci Technol 2023; 87: 104858.
http://dx.doi.org/10.1016/j.jddst.2023.104858

[31] Zacaron TM, Silva MLS, Costa MP, *et al.* Advancements in chitosan-based nanoparticles for pulmonary drug delivery. Polymers 2023; 15(18): 3849.
http://dx.doi.org/10.3390/polym15183849 PMID: 37765701

[32] Haseli S, Pourmadadi M, Samadi A, *et al.* A novel pH -responsive nanoniosomal emulsion for sustained release of curcumin from a chitosan-based nanocarrier: Emphasis on the concurrent improvement of loading, sustained release, and apoptosis induction. Biotechnol Prog 2022; 38(5): e3280.
http://dx.doi.org/10.1002/btpr.3280 PMID: 35678755

[33] Soni SS, D'Elia AM, Alsasa A, *et al.* Sustained release of drug-loaded nanoparticles from injectable hydrogels enables long-term control of macrophage phenotype. Biomater Sci 2022; 10(24): 6951-67.
http://dx.doi.org/10.1039/D2BM01113A PMID: 36341688

[34] Huang H, Lou Z, Zheng S, *et al.* Intra-articular drug delivery systems for osteoarthritis therapy: shifting from sustained release to enhancing penetration into cartilage. Drug Deliv 2022; 29(1): 767-91.
http://dx.doi.org/10.1080/10717544.2022.2048130 PMID: 35261301

[35] Yu DG, Wang M, Ge R. Strategies for sustained drug release from electrospun multi-layer nanostructures. Wiley Interdiscip Rev Nanomed Nanobiotechnol 2022; 14(3): e1772.
http://dx.doi.org/10.1002/wnan.1772 PMID: 34964277

[36] Abadi AJ, Mirzaei S, Mahabady MK, *et al.* Curcumin and its derivatives in cancer therapy: Potentiating antitumor activity of cisplatin and reducing side effects. Phytother Res 2022; 36(1): 189-213.
http://dx.doi.org/10.1002/ptr.7305 PMID: 34697839

[37] Herdiana Y, Wathoni N, Shamsuddin S, Muchtaridi M. Drug release study of the chitosan-based nanoparticles. Heliyon 2022; 8(1): e08674.
http://dx.doi.org/10.1016/j.heliyon.2021.e08674 PMID: 35028457

[38] Rosen DB, Kvarnhammar AM, Laufer B, *et al.* TransCon IL-2 β/γ: A novel long-acting prodrug with sustained release of an IL-2Rβ/γ-selective IL-2 variant with improved pharmacokinetics and potent activation of cytotoxic immune cells for the treatment of cancer. J Immunother Cancer 2022; 10(7): e004991.
http://dx.doi.org/10.1136/jitc-2022-004991 PMID: 35817480

[39] Yuan H, Zhang Z, Hu L. Development and characterization of gastro-floating sustained-release capsule with improved bioavailability of levodopa. Drug Deliv Transl Res 2023; 13(1): 9-17.
http://dx.doi.org/10.1007/s13346-022-01188-5 PMID: 35661106

[40] Gawade A, Polshettiwar S, Hingalajia H, Prajapati BG, Singh A. Pharmacokinetics and pharmacodynamics of various novel formulations targeting Alzheimer's disease. In: Alzheimer's Disease and Advanced Drug Delivery Strategies. Elsevier 2024; pp. 391-402.

[41] Kousar K, Naseer F, Abduh MS, *et al.* Green synthesis of hyaluronic acid coated, thiolated chitosan nanoparticles for CD44 targeted delivery and sustained release of Cisplatin in cervical carcinoma. Front Pharmacol 2023; 13: 1073004.
http://dx.doi.org/10.3389/fphar.2022.1073004 PMID: 36712656

[42] Sabzini M, Pourmadadi M, Yazdian F, Khadiv-Parsi P, Rashedi H. Development of chitosan/halloysite/graphitic-carbon nitride nanovehicle for targeted delivery of quercetin to enhance its limitation in cancer therapy: An *in vitro* cytotoxicity against MCF-7 cells. Int J Biol Macromol 2023; 226: 159-71.
http://dx.doi.org/10.1016/j.ijbiomac.2022.11.189 PMID: 36435458

[43] Kumar A, Yadav S, Pramanik J, *et al.* Chitosan-based composites: Development and perspective in food preservation and biomedical applications. Polymers 2023; 15(15): 3150.
http://dx.doi.org/10.3390/polym15153150 PMID: 37571044

[44] Al-Qubaisi MS, Al-Abboodi AS, Alhassan FH, *et al.* Preparation, characterization, *in vitro* drug release and anti-inflammatory of thymoquinone-loaded chitosan nanocomposite. Saudi Pharm J 2022; 30(4): 347-58.
http://dx.doi.org/10.1016/j.jsps.2022.02.002 PMID: 35527823

[45] Hussein-al-ali SH, Hussein MZ, Ayoub R, Fakurazi S, Abualassal QIA, Al-Dalahmeh Y. Development of new drug formulations: Cetirizine-polymers nanoparticles. Acta Pol Pharm 2021; 78(3)

[46] Abu Sharar AA, Ramadan SZ, Hussein-Al-Ali SH. Multiobjective optimization of fluphenazine nanocomposite formulation using NSGA-II method. Mater Sci Pol 2021; 39(4): 517-44.
http://dx.doi.org/10.2478/msp-2021-0042

[47] Prajapati BG, Jivani M, Paliwal H. Formulation and optimization of topical nanoemulsion based gel of mometasone furoate using 32 full factorial design. Indian Drugs 2021; 6(06): 19-29.

[48] Shah S, Ghetiya R, Soniwala M, Chavda J. Development and optimization of inhalable levofloxacin nanoparticles for the treatment of tuberculosis. Curr Drug Deliv 2021; 18(6): 779-93.

http://dx.doi.org/10.2174/1567201817999201103194626 PMID: 33155907

[49] El Baz AF, Shetaia YMH, Shams EHA, ElMekawy A. Optimization of cellulase production by Trichoderma viride using response surface methodology. Curr Biotechnol 2018; 7(1): 19-25. http://dx.doi.org/10.2174/2211550105666160115213402

[50] Kumari M, Gupta SK. Response surface methodological (RSM) approach for optimizing the removal of trihalomethanes (THMs) and its precursor's by surfactant modified magnetic nanoadsorbents (sMNP) - An endeavor to diminish probable cancer risk. Sci Rep 2019; 9(1): 18339. http://dx.doi.org/10.1038/s41598-019-54902-8 PMID: 31797998

[51] Huber L. Validation and qualification in analytical laboratories 2007.

[52] Allen TT, Allen TT. Software overview and methods review: Minitab: statistical quality control and design of experiments and systems. In: Introduction to Engineering Statistics and Lean Six Sigma. 2019; pp. 575-600.

[53] Lesik SA. Applied statistical inference with MINITAB. CRC Press 2018. http://dx.doi.org/10.1201/9780429444951

[54] Lewis-Beck MS, Skalaban A. The R-squared: Some straight talk. Polit Anal 1990; 2: 153-71. http://dx.doi.org/10.1093/pan/2.1.153

[55] Boylan GL, Cho BR. The normal probability plot as a tool for understanding data: A shape analysis from the perspective of skewness, kurtosis, and variability. Qual Reliab Eng Int 2012; 28(3): 249-64. http://dx.doi.org/10.1002/qre.1241

[56] Abul Kalam M, Khan AA, Khan S, Almalik A, Alshamsan A. Optimizing indomethacin-loaded chitosan nanoparticle size, encapsulation, and release using Box–Behnken experimental design. Int J Biol Macromol 2016; 87: 329-40. http://dx.doi.org/10.1016/j.ijbiomac.2016.02.033 PMID: 26893052

[57] Larsen WA, McCleary SJ. The use of partial residual plots in regression analysis. Technometrics 1972; 14(3): 781-90. http://dx.doi.org/10.1080/00401706.1972.10488966

[58] Tranmer M, Elliot M. Multiple linear regression. CMI 2008; 5(5): 1-5.

[59] Pokkalla DK, Wang Z, Teoh JC, Poh LH, Lim CT, Quek ST. Soft missing rib structures with controllable negative poisson's ratios over large strains *via* isogeometric design optimization. J Eng Mech 2022; 148(11): 04022063. http://dx.doi.org/10.1061/(ASCE)EM.1943-7889.0002149

[60] Lee R. Statistical design of experiments for screening and optimization. Chemieingenieurtechnik 2019; 91(3): 191-200. http://dx.doi.org/10.1002/cite.201800100

[61] Muley AB, Ladole MR, Suprasanna P, Dalvi SG. Intensification in biological properties of chitosan after γ-irradiation. Int J Biol Macromol 2019; 131: 435-44. http://dx.doi.org/10.1016/j.ijbiomac.2019.03.072 PMID: 30876903

[62] Anand M, Sathyapriya P, Maruthupandy M, Hameedha Beevi A. Synthesis of chitosan nanoparticles by TPP and their potential mosquito larvicidal application. Front Laborat Med 2018; 2(2): 72-8. http://dx.doi.org/10.1016/j.flm.2018.07.003

[63] Jia Z, Yang C, Zhao F, Chao X, Li Y, Xing H. One-step reinforcement and deacidification of paper documents: Application of Lewis base—Chitosan nanoparticle coatings and analytical characterization. Coatings 2020; 10(12): 1226. http://dx.doi.org/10.3390/coatings10121226

[64] Anwer MK, Fatima F, Ahmed MM, *et al*. Abemaciclib-loaded ethylcellulose based nanosponges for sustained cytotoxicity against MCF-7 and MDA-MB-231 human breast cancer cells lines. Saudi Pharm J 2022; 30(6): 726-34. http://dx.doi.org/10.1016/j.jsps.2022.03.019 PMID: 35812154

[65] Lei Z, Alwan M, Alamir HTA, *et al.* Detection of abemaciclib, an anti-breast cancer agent, using a new electrochemical DNA biosensor. Front Chem 2022; 10: 980162. http://dx.doi.org/10.3389/fchem.2022.980162 PMID: 36339035

[66] Khorsandi Z, Hajipour AR, Sarfjoo MR, Varma RS. A Pd/Cu-Free magnetic cobalt catalyst for C–N cross coupling reactions: Synthesis of abemaciclib and fedratinib. Green Chem 2021; 23(14): 5222-9. http://dx.doi.org/10.1039/D1GC00518A

[67] Lustriane C, Dwivany FM, Suendo V, Reza M. Effect of chitosan and chitosan-nanoparticles on post harvest quality of banana fruits. J Plant Biotechnol 2018; 45(1): 36-44. http://dx.doi.org/10.5010/JPB.2018.45.1.036

[68] Bhumkar DR, Pokharkar VB. Studies on effect of pH on cross-linking of chitosan with sodium tripolyphosphate: A technical note. AAPS PharmSciTech 2006; 7(2): E138-43. http://dx.doi.org/10.1208/pt070250 PMID: 16796367

[69] Karimi M, Avci P, Ahi M, Gazori T, Hamblin MR, Naderi-Manesh H. Evaluation of chitosan-tripolyphosphate nanoparticles as a p-shRNA delivery vector: formulation, optimization and cellular uptake study. J Nanopharm Drug Deliv 2013; 1(3): 266-78. http://dx.doi.org/10.1166/jnd.2013.1027 PMID: 26989641